

Clonally expanded effector CD4⁺ cytotoxic T lymphocytes are associated with severe neurological adverse events after immune checkpoint inhibitor therapy

Ambre Manon Giguelay , 1,2 Patrick Maschmeyer , 1,2,3 Leonie Müller-Jensen , 1,4 Christian Schinke, 1,4 Smilla K Maierhof, 1,4,5 Natasha Nambiar, 1,2 Manpreet Meyer , 1,2,6,7 Petra Huehnchen , 1,4,8 Wolfgang Boehmerle , 1,4,8 Matthias Endres , 1,4,8,9,10,11,12 Samuel Knauss, 1,4 Leif S. Ludwig 1,2

To cite: Giguelay AM, Maschmeyer P, Müller-Jensen L, et al. Clonally expanded effector CD4⁺ cytotoxic T lymphocytes are associated with severe neurological adverse events after immune checkpoint inhibitor therapy. *Journal for ImmunoTherapy of Cancer* 2025;**13**:e012350. doi:10.1136/ jitc-2025-012350

► Additional supplemental material is published online only. To view, please visit the journal online (https://doi.org/10.1136/jitc-2025-012350).

AMG and PM contributed equally.

AMG and PM are joint first authors.

SK and LSL are joint senior authors.

Accepted 14 September 2025



© Author(s) (or their employer(s)) 2025. Re-use permitted under CC BY-NC. No commercial re-use. See rights and permissions. Published by BMJ Group.

For numbered affiliations see end of article.

Correspondence to

Dr Leif S. Ludwig; leif.ludwig@bih-charite.de

Dr Samuel Knauss; samuel.knauss@charite.de

ABSTRACT

Background Immune checkpoint inhibitor (ICI) therapies present a pillar of modern cancer therapy but can cause neurological immune-related adverse events (n-irAEs), of which up to 35% are severe or even fatal. However, the detailed immunological mechanisms and risk factors underlying n-irAEs remain largely unknown. Here, we leveraged single-cell genomics to dissect immune cell type, state, and clonal heterogeneity associated with n-irAEs.

Methods We performed coupled single-cell RNA sequencing and T cell receptor (TCR) profiling on peripheral blood cells of 17 patients with cancer receiving ICI therapy, including 8 patients with acute neurotoxicity. This approach enabled integrated analyses of immune cell states and T cell clonality linked to ICI-induced n-irAEs. Results We profiled 186 435 immune cells and conducted pseudotime analyses, revealing that patients with n-irAEs, compared with controls, present with clonally expanded CD4+ cytotoxic T lymphocytes (CD4+ CTLs) with an n-irAEspecific effector gene expression profile. These T cells predominantly belong to a select set of expanded clonal families and express genes linked to antigen-induced activation, cell lysis, and neuroinflammation. Moreover, they highly express CXCR3 (FC=2.03 compared with control CD4⁺ CTLs, with a false discovery rate=7.7×10⁻⁴), encoding the chemokine receptor of CXCL10, previously nominated as a biomarker for severe ICI therapy-induced n-irAEs with concomitant multiple organ system toxicity. **Conclusions** Overall, our study highlights the expansion and activation of CD4+ CTLs in ICI-induced neurotoxicity. proposing these cells as potential targets for developing new biomarkers and therapeutic strategies to improve patient outcomes.

BACKGROUND

Immune checkpoint inhibitor (ICI) therapies have demonstrated remarkable efficacy in treating cancers and have become

WHAT IS ALREADY KNOWN ON THIS TOPIC

⇒ Neurological immune-related adverse events (nirAEs) often result in termination of immune checkpoint inhibitor (ICI) therapy, severe morbidity, or death. The critical molecular and cellular drivers of ICI-induced n-irAEs remain unknown.

WHAT THIS STUDY ADDS

⇒ Using single-cell RNA sequencing and T cell receptor profiling, we identify a clonally expanded subset of cytotoxic CD4⁺ T cells (CD4⁺ CTLs) with a distinct effector phenotype that is specifically present in patients with n-irAEs but not in ICI-treated control patients.

HOW THIS STUDY MIGHT AFFECT RESEARCH, PRACTICE OR POLICY

⇒ This study implicates a critical function of CD4⁺ CTLs in the manifestation of n-irAEs, warranting the investigation of targeting this population and/or its molecular mediators for therapeutic intervention of ICI-induced n-irAEs.

a cornerstone of contemporary oncology.¹ These treatments rely on antibody-mediated blocking of inhibitory T cell receptors, such as cytotoxic T lymphocyte-associated protein 4 (CTLA-4), programmed cell death protein 1 (PD-1), or programmed death-ligand 1 (PD-L1), which dampen T cell responses and augment tumor immune evasion.² Consequently, antibodies blocking these receptors enhance tumor clearance by modulating T cell activity to target malignant cells.¹²

However, the use of ICIs is associated with the development of often severe immunerelated adverse events (irAEs).³ IrAEs occur



in 54%-76% of patients receiving ICI treatment and can affect a wide range of organ systems.³ In 1%–3% of patients, irAEs affect the nervous system (neurologicalirAEs, n-irAEs) in diverse manifestations, including encephalitis and myositis. 4 Given the increasing number of ICI-treated patients, n-irAEs represent a significant clinical challenge, as they frequently cause severe pathologies or even death in up to 35% of cases. 4-7 Moreover, severe n-irAEs often require systemic immunosuppression and termination of ICI treatment, potentially favoring tumor outgrowth.⁸ Diagnosis and treatment of n-irAEs remain challenging due to their diverse clinical manifestations, the lack of reliable biomarkers, and an insufficient understanding of the underlying immunological mechanisms.⁹ Therefore, obtaining a deeper mechanistic insight into the development, prediction, and management of n-irAEs will be mandatory for the effective and safe use of ICI therapies.

To date, only a few studies have specifically focused on n-irAEs, but prior efforts have investigated T cell subset composition, effector phenotypes, and clonality more generally in irAEs. Notably, the degree of clonal diversity among different T cell subsets has been strongly linked to severe irAEs. These studies suggest a strong general impact of T cell phenotype and clonality on irAE manifestation. ¹⁰ 11 However, frequencies and types of T cell effector populations vary considerably between irAE-affected organ systems, demonstrating the need for neurotoxicity-focused efforts, which remain underdeveloped. 12 Regarding n-irAEs in particular, oligoclonal EBVspecific memory cytotoxic CD4⁺ T cell infiltrates were observed in a single case of fatal encephalitis following anti-PD-1 treatment. 13 Moreover, we recently detected elevated frequencies of CD8+ T memory cell subsets in n-irAE patients via mass cytometry. 14 However, we were limited in assessing detailed cell states and clonal information.

Here, we leveraged single-cell genomics-based profiling to characterize peripheral blood mononuclear cells (PBMCs) from patients with cancer developing ICI-induced n-irAEs. Most notably, we identified terminally differentiated CD4⁺ cytotoxic T lymphocytes (CD4⁺ CTLs) to substantially contribute to the pool of top expanded clonotypes, particularly in n-irAE patients. In those patients, the CD4⁺ CTLs display a strong effector phenotype, expressing genes indicative of recent TCR-mediated activation, cytotoxicity, and chemoattraction to inflammatory cytokines, suggesting a major role in the manifestation of n-irAEs.

METHODS Patient cohort

We enrolled adult patients with cancer with ICI-induced neurotoxicities treated at our center (Charité Universitätsmedizin Berlin) between September 2017 and December 2021. Patients receiving anti-PD-1, anti-PD-L1, or combination ICI treatment (anti-PD-1 + anti-CTLA-4)

were included. N-irAEs were diagnosed according to consensus criteria for "definite" or "probable" n-irAEs (online supplemental table 2). 15 Blood samples from n-irAE patients (n=8) were collected during the acute disease stage, with four patients receiving corticosteroids at the time of collection due to rapid clinical decline. As controls, we recruited consecutive cancer patients (n=9) scheduled for ICI treatment, matched for cancer type, ICI regimen, age, and sex where feasible (table 1, online supplemental table 2). Control patients with ICI treatment in the previous 6 months were excluded. Control group samples were collected before and 4-6 weeks after ICI treatment initiation. PBMCs were isolated using Vacutainer cell preparation tubes with sodium tubes (BD), according to protocol. Subsequently, isolated PBMCs were cryopreserved in 90% FBS and 10% dimethyl sulfoxide.

Single-cell RNA-seq and TCR-seq library preparation

Cryopreserved PBMCs were thawed at 37°C in a water bath, followed by serial dilution with prewarmed RPMI including 10% FBS. Cells were washed with FACS buffer (PBS+2% FBS) and centrifuged at 400xg for 5min at 4°C. Subsequently, Fc receptors were blocked (Human TruStain FcX, BioLegend) and stained on ice with anti-CD14-AF488 (clone 63D3, BioLegend), anti-CD66b-PE (clone G10F5, BioLegend) and SYTOX Blue (Thermo Fisher, S34857). After two additional washes, neutrophil depletion was achieved by sorting viable SYTOX Blue CD66b cells on a FACS Aria III flow sorter. Sorted cells were washed, centrifuged, and resuspended in Cell Suspension Buffer (PBS+0,04% BSA) and counted. Next, scRNA-seq and TCR-seq libraries were prepared by using 10x Genomics Chromium Next GEM Single Cell 5' Reagent Kits (v2) (CG000331 Rev D, individual kits specified in online supplemental table 1) according to the manufacturer's instructions. In brief, single-cellcontaining Gel Beads-in-emulsion (GEMs) were generated by loading suspended cells into a 10x Genomics Chromium Controller before reverse transcription and cDNA synthesis. TCR gene-containing cDNAs were amplified by two subsequent (semi-nested) PCRs. Amplified TCR cDNA and cDNA for gene expression (GEX) libraries were fragmented prior to end-repair, A-tailing, adaptor ligation, and indexing. All PCRs were performed using a C1000 Touch Thermal Cycler with 96-Deep Well Reaction Module (BioRad Laboratories). Quality assessment and concentration quantification of the final 5' GEX and TCR libraries were performed with Qubit and an Agilent BioAnalyzer.

Illumina sequencing of GEX and TCR libraries, preprocessing and quality control

10x Genomics 5' scRNA-seq GEX and TCR libraries were sequenced with the Illumina NovaSeq 6000 sequencing platform. All libraries were sequenced using a paired-end dual-indexing sequencing protocol with 26, 10, 10, 90 read lengths. Raw sequencing data were demultiplexed



Table 1 Overview of clinical characteristics in control and n-irAE patient groups

Demographics and general info	Control (n=9)	n-irAEs (n=8)
Median age (years, range)	62 (49–90)	64 (58–82)
Female patients	3 (33%)	2 (25%)
Cancer type (neoplasm)		
Melanoma	3 (33%)	1 (13%)
Lung cancer	4 (44%)	3 (33%)
Liver cancer	1 (11%)	1 (13%)
Merkel cell carcinoma	1 (11%)	2 (25%)
Prostate cancer	0 (0%)	1 (13%)
ICI treatment at therapy start		
PD-1 inhibitor	4 (44%)	2 (25%)
PD-L1 inhibitor	4 (44%)	4 (25%)
Combined PD-1/CTLA4 blockade	1 (11%)	2 (25%)
Neurological irAEs (n-irAEs)		
Myositis/myopathy	0 (0%)	7 (88%)
Peripheral neuropathy	0 (0%)	1 (13%)
Encephalitis	0 (0%)	2 (25%)
Myasthenic syndrome	0 (0%)	1 (13%)
Patients with multiple n-irAEs	0 (0%)	3 (38%)
Other irAEs (non-n-irAEs)		
Patients with non-n-irAEs at sampling	3 (33%)	6 (75%)
Clinical metadata		
Median time from ICI start to sample collection (weeks, range)	6 (4–6)	30 (5–207)
Corticosteroid treatment at time of sampling	0 (0%)	4 (50%)
Survival at 12 months post-ICI therapy start	8 (89%)	7 (88%)

This table summarizes clinical information for the control and n-irAE patient groups. Values are shown as medians with ranges or as counts with corresponding percentages, as indicated in the table.

ICI, immune checkpoint inhibitor; n-irAE, neurological immune-related adverse event.

using CellRanger mkfastq. Demultiplexed sequencing reads for all libraries were aligned to the reference genome GRCh38-2020-A using CellRanger Multi (cellranger-6.1.2) from 10x Genomics.

Data analysis

All the statistical analyses were performed using R V.4.2.2 (or R V.4.2.3 for the differential gene expression analysis (DGE)), and Seurat V.4.3.0.¹⁶ Population frequencies, pseudotime, area under the curves (AUC), and scores were compared with a Wilcoxon test (non-paired between the groups, control/n-irAE, or partially paired between pretreatment/post-treatment samples).

Low-quality cells were filtered out according to the following criteria: (1) mitochondrial content $\geq 10\%$, (2) ribosomal content $\geq 50\%$, (3) number of Unique Molecular Identifiers ≤ 2000 , and (4) number of detected genes ≤ 800 . Multiplets were identified with DoubletFinder¹⁷, accounting for homotypic doublets and estimating the expected doublet rate via a linear regression based on 10x Genomics' instructions. Datasets were then integrated with Seurat's anchor method on 2000 integration

features. Both uniform manifold approximation and projection (UMAPs) and clusterings were performed on the integrated data, except for the $\mathrm{CD4}^{\scriptscriptstyle +}$ CTL top clone-focused analyses (online supplemental figure 6), where the low cell numbers in some patients prevented proper integration.

Cell type assignment was first performed with an Azimuth¹⁶ PBMC reference dataset, followed by minor manual re-adjustment of some clusters according to marker GEX. In particular, clusters 21 and 27 were labeled low-quality cells, and the mixed clusters 10, 14, and 17, showing poor annotation prediction scores, were re-annotated as gamma delta T cells, Tregs, and CD4⁺ CTLs, respectively.

Because cell type assignment in discrete cell types does not necessarily reflect the continuous dimension of lymphocyte differentiation, pseudotime analysis with Slingshot¹⁸ was performed on CD4⁺ and CD8⁺ T cells. Before pseudotime inference, the respective subsets of the dataset were reintegrated as described above. In both cases, proliferating cells were excluded as their

transcriptome signature is dominated by cell cycle programs. For CD4⁺ T cells, Tregs were excluded, given that their differentiation trajectory is distinct from other effector cell populations developing from naive T cells. The pseudotime value presented corresponds to the value associated with the main branch. The proportion of cells from irAE patients as a function of pseudotime was calculated with a running window. To estimate the probability that such a proportion could be found by chance, we permuted 1000 times cell barcodes and evaluated the proportion obtained for each permutation. Then, the 2.5% and 97.5% quantiles were calculated at each pseudotime point, forming a 95% CI. Reassuringly, for each lymphocyte compartment, this CI is very stable over pseudotime and centered on the global proportion of irAE cells.

Exhaustion, naivety, and cytotoxicity scores were calculated with AUCells¹⁹, based on the expression of the following genes:

Exhaustion	CTLA4, TIGIT, PD1, LAG3, TIM3
Cytotoxicity	NKG7, CCL4, CST7, PRF1, GZMA, GZMB, IFNG, CCL3, FGFBP2
Naivety	CCR7, LEF1, SELL

Their value along pseudotime was smoothed as described above.

TCR analysis was conducted in both CD4⁺ and CD8⁺ T cell compartments independently. Subpopulation enrichment of the top 10 expanded clones was assessed with a hypergeometric test. That is, the proportion of a specific subpopulation in each top clone was compared with its proportion in the whole set of CD4⁺ or CD8⁺ T cells of the respective patient. A score directly based on the p value associated with the statistical test (min(-log10(p value), 16)) was then used to compare the enrichment between the control and irAE groups. Thus, a score below 2 would indicate no enrichment of the subpopulation. Because only expanded clones (ie, clones detected at least twice in the respective cell population) were considered for this analysis, each patient was represented by 0–10 clones. Here, we note that using a maximum value (16) is due to an artificial limit of the package that affects comparing the extent of cell type bias in the two patient groups. For example, the cell type bias in the n-irAE group is likely to be underestimated, with the biological conclusions remaining unchanged.

DGE analysis was performed via pseudobulk at the clonotype level with *edgeR*. P values were corrected for multiple testing with the Benjamini-Hochberg method. Z-scores of the most significant (adjusted p<0.01 and absolute fold change >1.5) differentially expressed genes were averaged at the clonotype resolution for heatmap representation and principal component analysis (PCA). Genes encoding the variable domain of the TCR were excluded since they are clonotype-specific by definition. PCA was also calculated at the cell level. The same set of genes was then used to define the control group and

n-irAE group signature, whose scores were computed with AUCell.²¹ The Gene Ontology (GO) term Over Representation Analysis was conducted with the R package *clusterProfiler*, calculating Benjamini-Hochberg q-values, on genes expressed in at least three different patients and with an average greater than 0.2 in at least 5% of the different clonotypes.

This case–control study was reported in accordance with the Strengthening the Reporting of Observational Studies in Epidemiology guidelines.²⁰

RESULTS

Single-cell and TCR profiling of the immune landscape of ICItreated patients with and without n-irAEs

To investigate potential alterations in blood cell type composition, cell states, and T lymphocyte clonality associated with severe ICI-induced n-irAEs, we performed single-cell RNA sequencing (scRNA-seq) with concomitant T cell receptor (TCR) profiling of PBMCs from two groups of ICI-treated patients presenting with (n=8; n-irAE group) or without (n=9; control group) n-irAEs (figure 1A, online supplemental figure 1, table 1, and online supplemental table 2).

After library preparation, sequencing, and data processing, 186435 cells met our quality control criteria (figure 1B and online supplemental figure 2A and B). No substantial differences in quality metrics and apparent batch effects of individual samples were observed after commonly applied qualitative assessment of integration and UMAP projection. The label transfer-based cell type annotation (online supplemental figure 2C-F) yielded all major blood cell types, expressing respective marker genes (figure 1B, online supplemental figure 2G). All major cell types were detected in samples (1), both before and after ICI treatment (online supplemental figure 2H), (2), both in the control and n-irAE groups (online supplemental figure 2I), and (3), spanning all cancer entities represented in the cohort (online supplemental figure 2J). Moreover, detected TCR sequences were confined to the alpha-beta T cell compartment (figure 1C). Together, this dataset provides a highresolution single-cell atlas of peripheral immune states and T cell clonality associated with ICI-induced n-irAEs in a clinically well-characterized patient cohort.

Immune cell subset analysis identifies minor frequency shifts associated with n-irAEs

On closer examination of immune cell subsets (online supplemental figure 3), we discerned a statistically significant (p<0.05) enrichment of CD4⁺ regulatory T cells (Tregs) in n-irAE patients compared with controls (median fold change (MFC) of 1.35; online supplemental figure 3B). Moreover, there was a non-significant but noticeable elevation in the frequencies of CD4⁺ CTLs (2.91 MFC, n.s.), proliferating CD4⁺ (1.7 MFC, n.s.) and

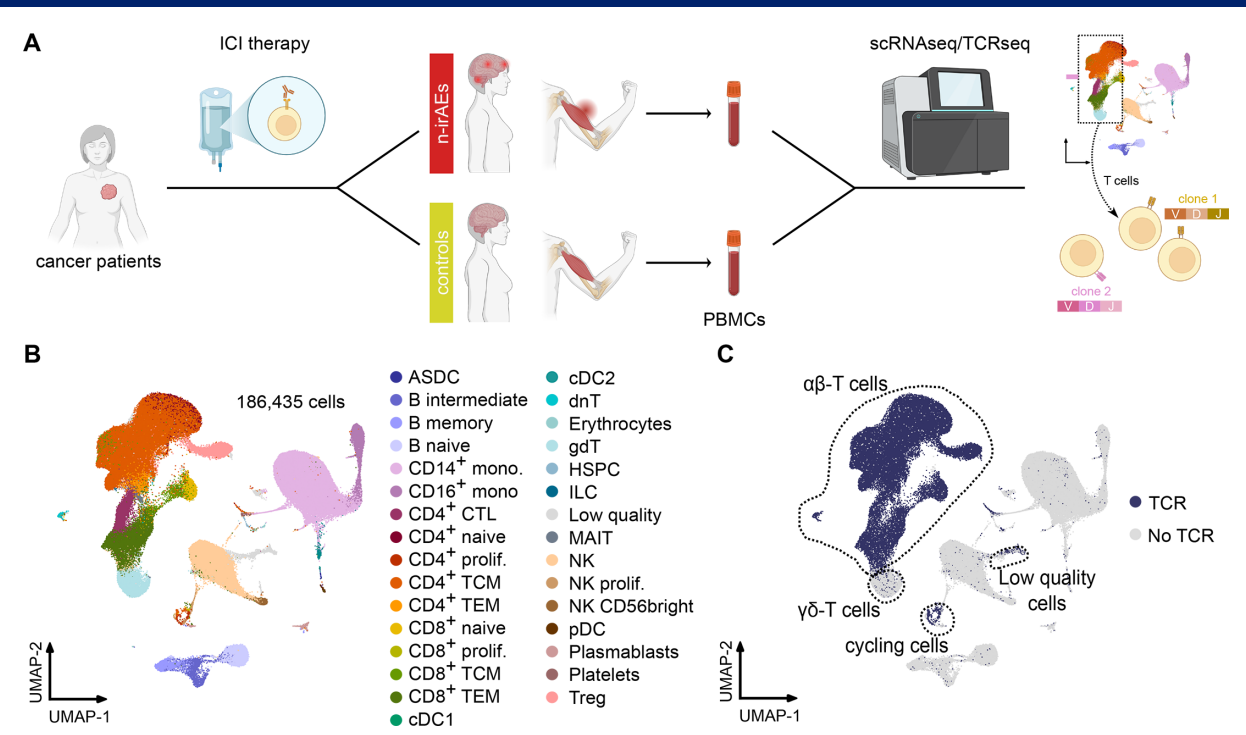


Figure 1 Immune cell profiling of ICI-treated cancer patients by combined single-cell RNA- and TCR-sequencing.

(A) Experimental workflow showing the collection of peripheral blood from ICI-treated cancer patients and processing of cells by scRNA-seq and TCR profiling. (B) UMAP projection of 186 435 PBMCs from ICI-treated patients with (n=8; n-irAEs) and without (n=9; controls) manifestation of neuroinflammation. (C) UMAP projecting the cells with (blue) or without (gray) detected TCR sequences. ICI, immune checkpoint inhibitor; n-irAEs, neurological immune-related adverse events; PBMCs, peripheral blood mononuclear cells; UMAP, uniform manifold approximation and projection.

CD8⁺ T cells, and CD8⁺ T central memory (TCM) cells (3.16, n.s.) in the n-irAE group (online supplemental figure 3B and C). Conversely, a trend toward diminished frequencies of CD4⁺ T effector/memory (TEM) cells (0.75 MFC, n.s.) and naive CD8⁺ T cells (0.43 MFC, n.s.) was evident in n-irAE patients when compared with controls (online supplemental figure 3B and C).

Moreover, we observed a shift in the differentiation state of circulating B cells in n-irAE patients, characterized by a skewing toward less differentiated cell types. Specifically, patients with n-irAEs showed increased frequencies of naive B cells, accompanied by a reduction in more differentiated subsets (online supplemental figure 3D). This included a statistically significant decrease in intermediate B cells, along with non-significant trends toward lower frequencies of memory B cells and plasmablasts. These changes collectively resulted in a lower B cell maturity score in n-irAE patients, with an MFC of 0.52 compared with the control group, although this difference did not reach statistical significance (online supplemental figure 3E). Notably, this skewing toward immature B cell states was not observed in control patients when comparing samples before and after ICI treatment, suggesting that the observed maturational shift is associated with n-irAE development rather than ICI therapy itself (online supplemental figure 3E). Overall, frequency analyses of discretely annotated immune cell subsets between n-irAE and

control patients highlighted only minor differences in immune cell type composition.

The most expanded T cell clones are confined to CD4⁺ CTLs and CD8⁺ TEM cells

Clonal T cell expansion is a substantial driver of irAEs after ICI therapy. We used TCR profiling to determine the top 10 most expanded clonotypes among CD4⁺ and CD8⁺ T cells and projected them on a UMAP of subsetted T cells to determine their distribution among T cell populations. Notably, the top expanded CD4⁺ and CD8⁺ T cell clones were nearly exclusively confined to CD4⁺ CTLs (figure 2A) and CD8⁺ TEM cells (figure 2B), respectively.

To quantify the extent of cell type bias within the 10 most expanded clones, we computed an enrichment score for each of them based on the p value of a hypergeometric test (Methods). For CD4⁺ CTLs, the score was greater than 2 in numerous clonotypes, indicating that in both patient groups, expanded clones were enriched in CD4⁺ CTLs in comparison to the whole CD4⁺ T cell population (figure 2C). Notably, this enrichment was significantly higher in n-irAE patients (median of 0 and 2.52 for the control and the n-irAE group, respectively), indicating a disproportionate expansion of CD4⁺ CTLs in patients with n-irAEs. In contrast, the same score calculated for CD4⁺ TCM cells showed no enrichment for this particular population (score <2; figure 2D), suggesting a more balanced distribution of expanded clones in this subset. Similarly, we observed a clonal enrichment specifically for

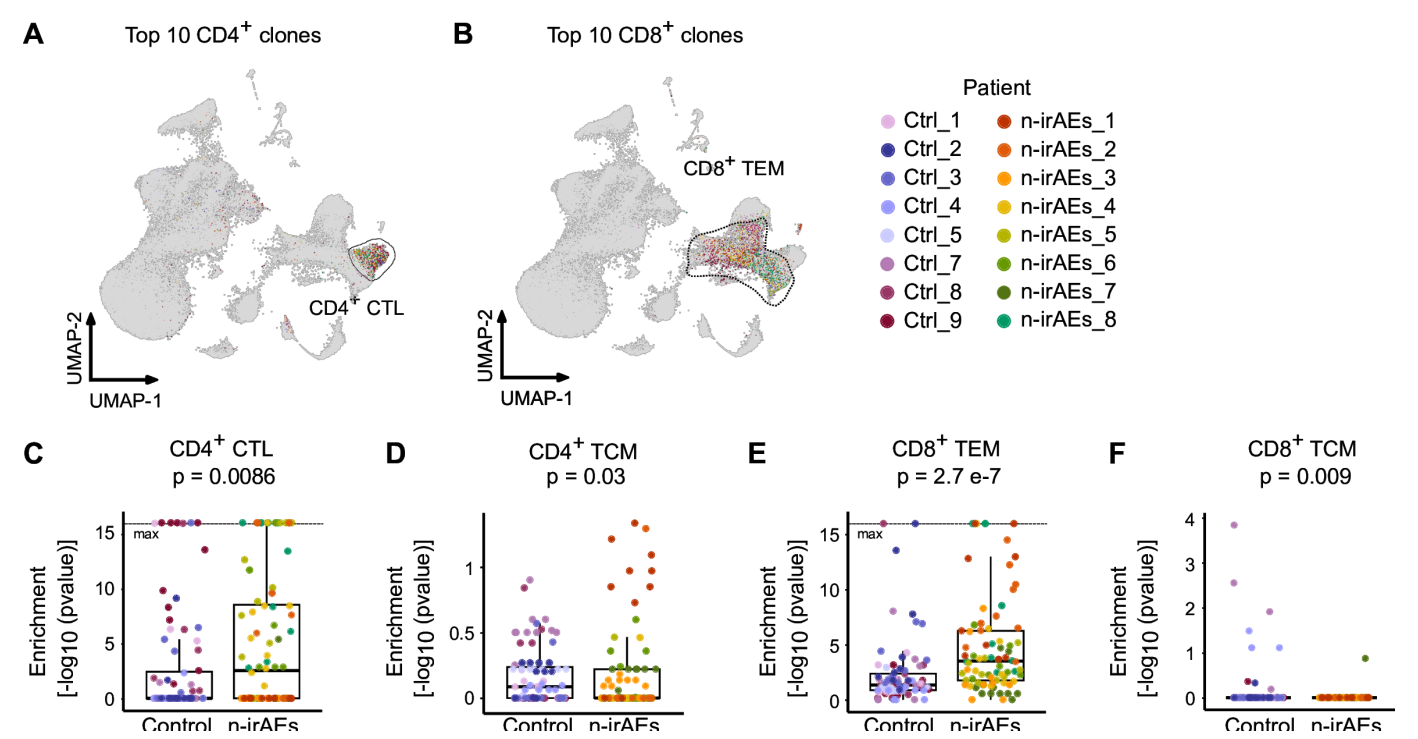


Figure 2 The most expanded T cell clones in n-irAE patients are strongly enriched in CD8⁺ TEM cells and CD4⁺ CTLs. (A, B) UMAP projection of the top 10 CD4⁺ (A) and CD8⁺ (B) T cell clones. (C–F) Enrichment score of CD4⁺ CTLs (C), CD4⁺ TCM (D), CD8⁺ TEM (E), and CD8⁺ TCM (F) cells for the top 10 expanded clones of each patient. The CD4⁺ and CD8⁺ T cell clones were analyzed separately. A score higher than 2 indicates a significant enrichment. P values correspond to a Wilcoxon test. n-irAE, neurological immune-related adverse event; UMAP, uniform manifold approximation and projection.

CD8⁺ TEM, but not for CD8⁺ TCM cells. Taken together, analysis of the most expanded clones within the CD4⁺ and CD8⁺ T cell compartments revealed a specific enrichment of these clones in CD4⁺ CTLs and CD8⁺ TEM cells, with a disproportionate accumulation observed particularly in n-irAE patients.

Terminally differentiated CD4⁺ CTL frequencies are increased in ICI-treated n-irAE patients

Analysis of cell type frequencies revealed only minor differences between patient groups (online supplemental figure 3), but may miss enrichment of specific cell states due to the limited resolution of this categorical approach. Thus, we applied Slingshot¹⁸ trajectory analysis to capture phenotypic shifts in T cell states along a continuum of differentiation, enabling a more refined assessment of subset enrichment in n-irAE versus control patients.

We first analyzed differentiation trajectories of conventional (ie, non-Treg) CD4⁺ T cells (figure 3A). The inferred trajectories followed the anticipated progression through discretely annotated cell populations, starting from naive T cells and transitioning through memory states at higher pseudotime values (figure 3B, online supplemental figure 4A). Notably, CD4⁺ CTLs were positioned farthest from naive cells along the trajectory, indicating a terminally differentiated phenotype (figure 3B, online supplemental figure 4A). Functional signature analysis further supported the cytotoxic character of these cells, showing that CD4⁺ CTLs exhibited the lowest naivety and the highest cytotoxicity

AUCell scores¹⁹ (figure 3C, online supplemental figure 4D). When comparing patient groups, naive CD4⁺ T cells from n-irAE patients displayed a lower naivety score, while CD4⁺ CTLs from these patients showed elevated pseudotime and cytotoxicity scores (online supplemental figure 4B-D). Most importantly, when comparing the contribution of patient cells along the trajectory in our integrated dataset, we found a pronounced enrichment of n-irAE patient cells at later pseudotime stages (~35), corresponding to CD4⁺ CTLs. In this region, the contribution of n-irAE patient-derived cells reached up to 70%, significantly exceeding their overall representation within the CD4⁺ T cell pool (46%) (figure 3D, online supplemental figure 4B). Notably, one control patient (Ctrl. 9) harbored more CD4⁺ CTLs than all other control patients combined (online supplemental figure 4B and F). The high abundance of CD4⁺ CTLs in this patient, however, was unrelated to ICI treatment or n-irAE development, as elevated CD4⁺ CTL frequencies were already present prior to treatment with checkpoint inhibitors (online supplemental figure 4F). Excluding this patient from the analysis revealed an even more pronounced difference in the contribution of cells from n-irAE versus control patients to the CD4⁺ CTL compartment (online supplemental figure 4E). Taken together, the most expanded CD4⁺ T cell clones were strongly biased toward CD4⁺ CTLs, particularly in n-irAE patients. Moreover, CD4⁺ CTLs were significantly enriched in cells derived from n-irAE patients, strongly indicating clonal expansion.

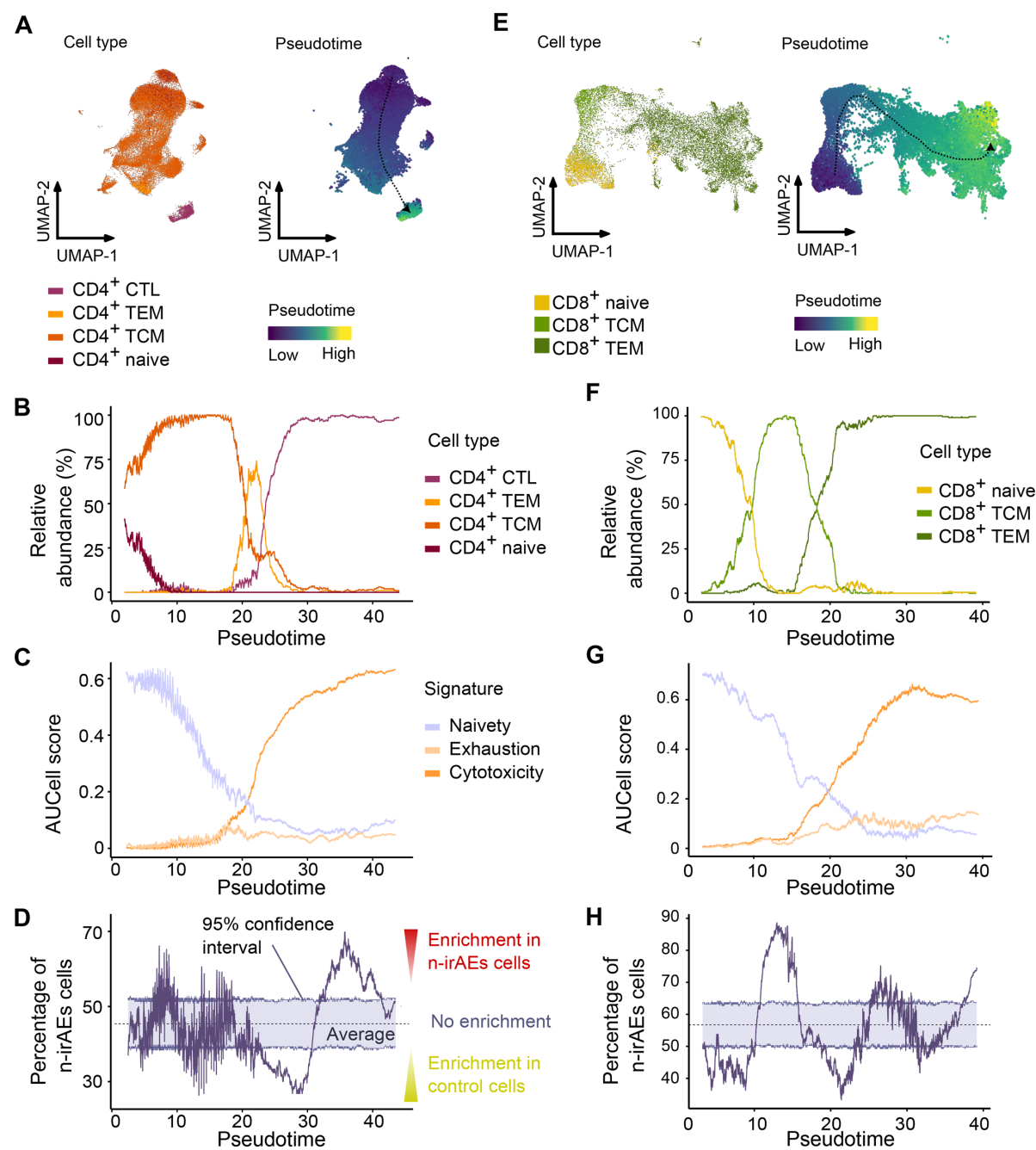


Figure 3 Pseudotime analysis of T cell subsets reveals an enrichment bias of n-irAE patient cells toward CD4⁺ CTLs. (A–D) Subsetting of CD4⁺ naive, central memory, effector/memory, and CTL cells (47 650 cells). (E–H) Subsetting of CD8⁺ *naïve*, central memory, and effector/memory cells (15 543 cells). (A, E) UMAP projections of the cell type annotation (left) and the pseudotime values (right). Proportion of the different cell types (B, F), *naïveté*, cytotoxicity, and exhaustion AUCell scores (C, G), and proportion of cells from n-irAE patients (D, H) are shown as a function of pseudotime, calculated on a sliding window. For Slingshot pseudotime analyses (B–D, F–H), only cells assigned to the main pseudotime branch were included (36 640 CD4⁺ T cells and 15 218 CD8⁺ T cells). The 95% CI after group assignment permutation is shown in D, H. AUC, area under the curve; n-irAE, neurological immune-related adverse events; UMAP, uniform manifold approximation and projection.

Next, we analyzed the differentiation trajectories of CD8⁺ T cells (figure 3E). Analogous to the trajectory analysis of CD4⁺ T cells, the inferred trajectories of CD8⁺ T cells aligned with the expected progression through discretely annotated subsets, starting with naive CD8⁺ T cells at low pseudotime values (<10) prior to transitioning through CD8⁺ TCM cells at intermediate stages (pseudotime value ~15), and culminating in CD8⁺ TEM

cells at the highest pseudotime values (>20) (figure 3F, online supplemental figure 5A). Accordingly, AUCell scores¹⁹ for naivety declined along the differentiation trajectory, while cytotoxicity and (to a lesser degree) exhaustion scores gradually increased with pseudotime (figure 3G, online supplemental figure 5C). When comparing patient group contributions of cells along the trajectory, naive CD8⁺ T cells with a low pseudotime score

were significantly enriched in cells derived from control patients (figure 3H, online supplemental figure 5B). In contrast, TCM cells were enriched with n-irAE cells, while CD8⁺ TEM cells that dominated the most expanded CD8⁺ T cell clones were not enriched with cells of any particular patient group (figure 2B and E, figure 3H, online supplemental figure 5B).

Highly expanded CD4⁺ CTL clonotypes in n-irAE patients possess a neuroinflammatory and cytotoxic effector phenotype

In contrast to CD8⁺ TEM cells, CD4⁺ CTLs did not only constitute the majority of the most expanded CD4⁺ T cell clones but were also enriched in cells derived from n-irAE patients, suggesting a role in n-irAE pathogenesis. Therefore, we sought to characterize the phenotypical differences of this subset between n-irAE and control patients.

After subsetting, CD4⁺ CTLs formed distinct clusters not only by patient group, but also by individual, reflecting substantial inter-patient heterogeneity (figure 4A). Subsequent unbiased differential GEX analysis of the top 10 expanded CD4⁺ CTL clones consistently revealed n-irAE-specific upregulation of genes involved in T cell activation $(CD69^{22}, HLA-DR^{23})$, effector cellassociated metabolic activity (SLC1A5²⁴), and genes that previously have been reported to be involved in neurological or muscular inflammation (DUSP1²⁵, FKBP5²⁶ ²⁷, HLA-DRB1²⁷, NR4A2²⁸, SMAP2²⁹; figure 4B and C, online supplemental figure 6A, online supplemental table 3). Interestingly, clonally expanded n-irAE CD4⁺ CTLs also significantly upregulated expression of the T cell trafficking receptor gene CXCR3 (FC=2.03, false discovery rate (FDR)= 7.7×10^{-4} ; figure 4B,C). Notably, CXCR3 is the receptor for CXCL10³⁰, which we have previously found at elevated serum concentrations and to be indicative of severe n-irAEs with multiorgan involvement. ¹⁴ In contrast, genes that were upregulated in the control group (mostly dominated by the previously identified "outlier" patient) included genes involved in homeostasis/cellular maintenance (eg, RPS26³¹, RPS27L³²) or exhaustion and apoptosis-associated genes (eg, TIGIT³³, FAS³⁴).

PCA of the significantly differentially expressed genes clearly separated the two patient groups, both at cell and clonotype resolution (online supplemental figure 6B). Moreover, similar results were achieved when using group signature scoring (figure 4D, online supplemental figure 6C), and control group and n-irAE group signatures were both significantly higher in their respective groups (figure 4E, online supplemental figure 6D). Finally, GO term enrichment analysis of activated genes confirmed the upregulation of pathways of key importance in antigen-stimulated CD4+ T cell activation and differentiation (figure 4F, online supplemental figure 6E). Of note, an analogous analysis of CD8+ TEM cells showed similar, but less distinct patterns of effector phenotypes between the two patient groups (online supplemental figure 7), corroborating the specificity of this observation for CD4⁺ T cells. Collectively, these results provide strong

supporting evidence for a causal contribution of clonally expanded CD4⁺ CTLs with an enhanced effector phenotype surrounding the development of n-irAEs.

DISCUSSION

ICI therapies have revolutionized cancer treatment, but they often (~21%) cause severe side effects across different organ systems, forcing treatment cessation.³⁵ Therefore, an intensive search for irAE biomarkers is underway to improve patient outcomes and therapies. Here, we employed scRNA-seq to determine immune cell states, frequencies, and T cell clonality, providing a comprehensive examination of these parameters in the context of n-irAEs. Through this analysis, we identified clonally expanded, terminally differentiated, CD4⁺ CTLs with an effector phenotype in the peripheral blood to be a characteristic feature of ICI-treated patients with severe n-irAEs.

Among immune cell subsets, CD8⁺ T cells have previously been implicated in irAE pathogenesis. 21 36 In our dataset, the most expanded CD8+ T cell clones were predominantly localized within the CD8⁺ TEM cell subset, with this pattern being particularly pronounced in n-irAE patients. However, we did not observe increased frequencies of CD8⁺ TEM cells in the blood of n-irAE patients, nor an enrichment of n-irAE-derived cells among CD8+ TEM cells along the differentiation trajectory of CD8⁺ T cells. The absence of detectable accumulation of clonally expanded CD8⁺ TEM cells in the circulation may be influenced by confounding factors such as sampling time points, underlying cancer types, or treatment regimens and does not exclude a pathogenic role of these cells in n-irAE manifestation, as they may have preferentially migrated into affected tumor and nervous tissues. However, their lack of enrichment in peripheral blood complicates their utility as accessible biomarkers for monitoring or predicting n-irAE development. Finally, while we observed differences in the GEX patterns between n-irAE and control CD8⁺ TEM cells, these differences were not very pronounced, also limiting the potential to identify molecular targets among this subset for the assessment or intervention of n-irAEs.

Besides CD8⁺ T cells, CD4⁺ T cells have gained attention as drivers of irAEs, given recent reports have (1) described their clonal expansion in irAEs and (2) suggested shared epitope expression between tumors and irAE-affected tissues, indicating T cell cross-reactivity as a potential mechanism of irAE development. ¹⁰ ^{37–39} In our dataset, the most expanded CD4⁺ T cell clones predominantly comprised CD4⁺ CTLs (figure 2A), likely reflecting a direct effect of ICI therapy, in line with previous reports. ⁴⁰ ⁴¹ Notably, this cell type bias toward the CD4⁺ CTL subset was even stronger in n-irAE patients (median enrichment score of 2.52; figure 2C) than in controls (median enrichment score of 0; figure 2C), suggesting the importance of CD4⁺ CTLs in the biological processes underlying n-irAEs. Moreover, we observed

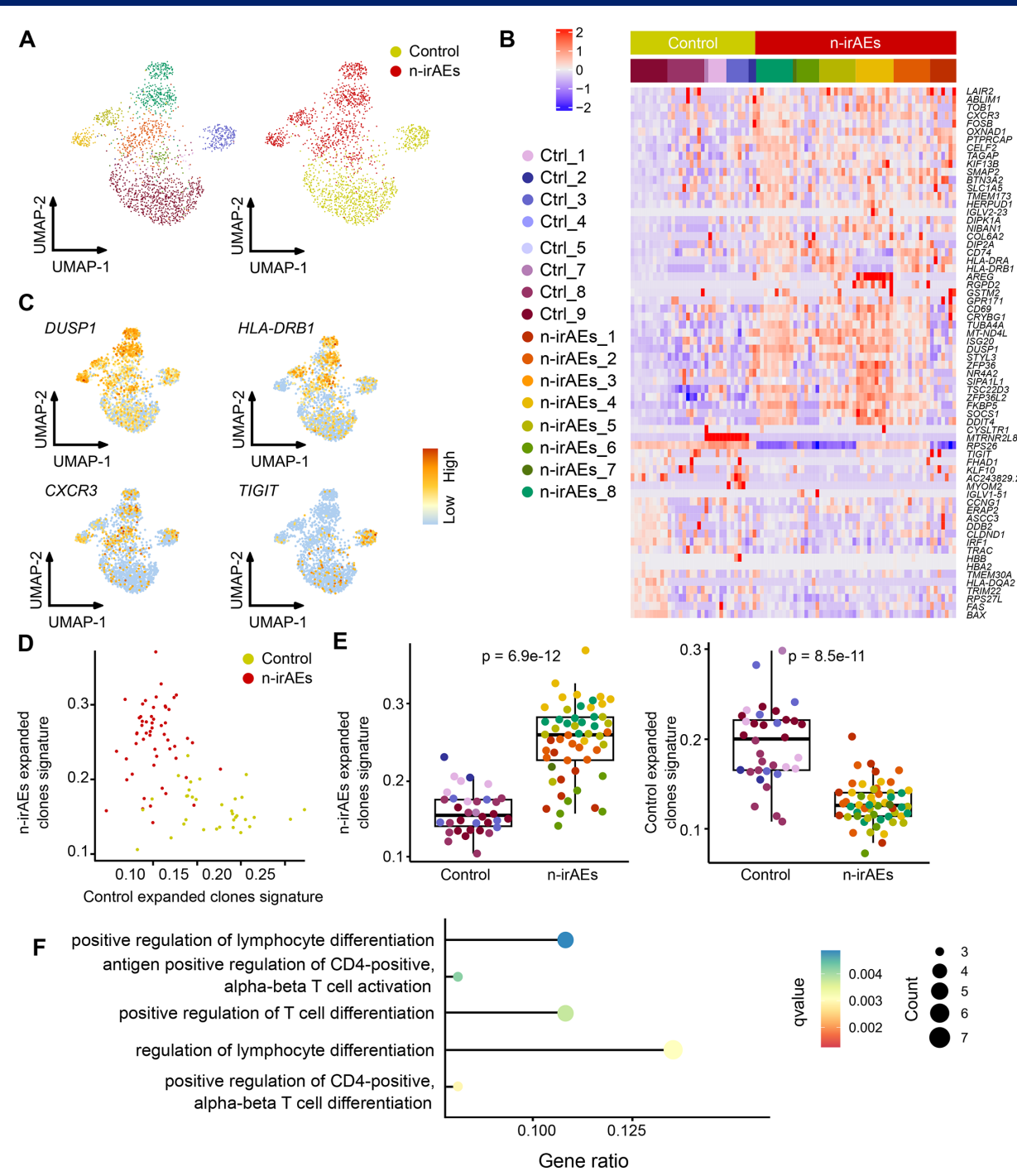


Figure 4 N-irAE CD4⁺ CTL top clones display altered transcriptomic profiles. (A) UMAP of the 1956 cells belonging to the CD4⁺ CTL top 10 clones, projecting the patient origin (left) and the patient group (right). (B) Heatmap showing the clone-wise pseudobulk expression of genes differentially expressed between the CD4⁺ CTL top clones from the control and n-irAE groups. (C) The normalized expression of indicated genes differentially expressed between the two groups is shown. (D, E) Scatter (D) and box plots (E) displaying the AUCell scores of signatures based on the genes shown in (B) for both control and n-irAE groups. The scores were calculated at the pseudobulk level per clone. (F) Selection of Gene Ontology Biological Processes (GOBP) highlighted by over-representation analysis of the n-irAE genes shown in (B). The dot diameters represent the number of genes overexpressed in the n-irAE top clones present in the GOBP. This number is then divided by the size of the GOBP to obtain the gene ratio. Q-values correspond to a hypergeometric test, after Benjamini-Hochberg correction. In (E) p values correspond to a Wilcoxon test. AUC, area under the curve; n-irAE, neurological immune-related adverse events; UMAP, uniform manifold approximation and projection.

a trend toward an up to threefold increase in CD4⁺ CTLs in n-irAE patients (online supplemental figure 3B), along with a significant (p<0.05) accumulation of up to

70% of n-irAE-derived cells specifically within the CD4⁺ CTL population along the CD4⁺ T cell differentiation trajectory (figure 3D). Together, these findings position

clonally expanded CD4⁺ CTLs as a key effector population in n-irAEs, potentially driven and amplified by autoor cross-reactivity to autoantigens of the nervous system. In the context of n-irAEs, cross-reactivity would require CD4⁺ CTLs to recognize antigens shared between tumors and nervous tissue, and to infiltrate both sites. Of note, it has been demonstrated that malignant cells can express MHC class II molecules, which is a requirement for CD4⁺ CTLs to lyse their target cells. 42-44 Moreover, CD4⁺ CTLs have been shown to infiltrate tumors, lyse malignant cells, and mediate immunity against cancers. 40 45 46 However, they have also been found to infiltrate the brain tissue of multiple sclerosis patients to exacerbate pathological inflammation.⁴⁷ Our results now suggest a direct link between ICI-mediated amplification of CD4⁺ CTLs for efficient tumor responses and neurotoxic side effects, potentially mediated by cross-reactivity between tumor and nervous tissue antigens. Further, they incentivize antigen screenings and functional assays on blood CD4⁺ CTLs from n-irAE patients to identify antigens that facilitate the auto-reactivity of these cells, similar to what has been done for CD8⁺ T cells in ICI-induced myocarditis.⁴⁸

Regarding the phenotype of CD4⁺ CTLs, cells from n-irAE patients possessed a higher cytotoxicity score than cells from the patient control group (online supplemental figure 4D), which includes cytolytic hallmark genes, such as Perforin1 (PRF1) and granzymes (GZMA, GZMB). 49 The top 10 expanded clones of n-irAE patients further exhibited elevated gene sets involved in T cell activation, differentiation, and effector function, as well as genes that contribute to neurological or muscular inflammation. Importantly, while we were able to detect expanded CD4⁺ CTL clones also in patients (mostly originating from one patient) without n-irAEs, these cells did not display such an activated effector phenotype. Moreover, we were able to deduce a GEX signature specific for n-irAE CD4⁺ CTLs, representing the potential to derive biomarkers for ICIinduced n-irAEs from blood samples.

Further studies are required to substantiate the neurotoxic function of CD4⁺ CTLs in n-irAE patients in situ. However, in n-irAE-associated CD4⁺ CTLs, CXCR3 transcripts were twofold upregulated (FDR=7.7×10⁻⁴) compared with control CD4⁺ CTLs, encoding the receptor of the CXCL9/10/11 chemokines²⁶ (figure 4B, online supplemental table 3). CXCL10 is expressed by immune and endothelial cells at inflammatory sites with the primary function to recruit CXCR3-expressing immune cells from the blood into inflamed tissues.³⁰ Importantly, in a previous masscytometry-centered study of a large patient cohort (n=83), we identified CXCL10 as a prominent indicator for ICI-induced high-grade neurotoxicity, also affecting other organ systems.¹⁴ Thus, expression of CXCR3 on blood CD4⁺ CTLs provides a direct link between the identification of CXCL10 as a biomarker for severe adverse events and a mechanism of action for pathological inflammation in nervous tissues or even multiple organ systems. Our results are further

noteworthy, given the report of a fatal case of ICI-induced encephalitis, where an oligoclonal cytotoxic CD4⁺ T cell population was identified in the brain. ¹³

Taken together, our results suggest for the first time the involvement of inflammation-tropic, expanded, and activated CD4⁺ CTL population in n-irAE patients following ICI therapy. Detectable in the peripheral blood, this population could be relevant for prediction, although future work will be needed to validate its use as a biomarker upstream of the first symptom development. These findings motivate in-depth investigations focusing on CD4⁺ CTL dynamics, including their presence already before ICI treatment and their modulation during therapy and emerging/manifested n-irAEs. Specifically, their presence may qualify as a patient-specific risk factor for developing n-irAEs and could guide early and late intervention, for example, by targeting CD4⁺ CTL function or migration to inflamed neurological tissues. In conclusion, we identify a clinically relevant CD4⁺ CTL subset surrounding n-irAEs, which further opens up novel possible treatment avenues to improve the clinical outcome of cancer patients with n-irAEs following ICI therapy.

Limitations of the study

Despite their clinical relevance, the relatively rare occurrence of n-irAEs substantially challenged the constitution of a large and homogeneous group of patients. Future efforts will be required to substantiate these findings in larger cohorts stratified by the type of neurological manifestation, collection time points, and associated treatments to further resolve additional pathophysiologic heterogeneity and longitudinal dynamics of n-irAE development and resolution. Further, PBMCs do not present the primary site of clinical relevance. Future efforts will be required to directly investigate immune cell characteristics in the affected tissue (e.g., cerebrospinal fluid, muscle biopsies).

Author affiliations

¹Berlin Institute of Health at Charité - Universitätsmedizin Berlin, Berlin, Germany ²Max-Delbrück-Center for Molecular Medicine in the Helmholtz Association (MDC), Berlin Institute for Medical Systems Biology (BIMSB), Berlin, Germany

³Institute for Systemic Inflammation Research (ISEF), University of Lübeck, Lübeck, Germany

⁴Department of Neurology with Experimental Neurology, Charité -

Universitätsmedizin Berlin, Berlin, Germany

⁵Einstein Center for Neurosciences Berlin (ECN) at Charité - Universitätsmedizin Berlin, Berlin, Germany

⁶Department of Biology, Chemistry, Pharmacy, Freie Universität Berlin, Berlin, Germany

⁷Boston Children's Hospital and Harvard Medical School, Boston, Massachusetts, USA

⁸NeuroCure Cluster of Excellence, Charité Universitätsmedizin Berlin, Berlin, Germany

⁹Charité Universitätsmedizin Berlin, Center for Stroke Research Berlin, Berlin, Germany

¹⁰German Center for Neurodegenerative Diseases (DZNE), partner site Berlin, Berlin, Germany

¹¹German Centre for Cardiovascular Research (DZHK), partner site Berlin, Berlin, Germany

¹²German Center for Mental Health (DZPG), partner site Berlin, Berlin, Germany



Acknowledgements We thank the MDC/BIH Genomics Platform, Berlin (Facility ID: 1565, The CoreMarketplace: MDC & BIH Technology Platform Genomics) for expert technical support and sequencing services, in particular Jeannine Wilde, Dr Tatiana Borodina, Dr Clemens Messerschmidt, and Dr Marten Jäger. We are grateful to Michaela Seeger-Zografakis and Caroline Braeuning from the Flow Cytometry Team of the MDC/BIH Genomics Technology Platform in the Helmholtz Association for their technical support. Computational analyses were performed on the high-performance computing (HPC) cluster of the Berlin Institute of Health. Finally, we thank the members of the Department of Neurology with Experimental Neurology and the Ludwig lab for their valuable input and fruitful discussions.

Contributors AMG, PM, SK and LSL conceived and designed this work. AMG led all data analyses and is responsible for the accuracy and reproducibility of the manuscript. PM performed genomics experiments and contributed to data analysis and interpretation. NN and MM aided in performing genomics experiments. LM-J, CS, SKM, PH, WB, ME and SK contributed to patient sample acquisition and/or provided clinical insights as well as critical comments in the manuscript. AMG, PM, SK and LSL wrote the paper with input from all authors. LSL is the guarantor of the work and had full access to all the data in the study and takes responsibility for the integrity of the data and the accuracy of the data analysis. We occasionally used ChatGPT during manuscript preparation to explore alternative phrasings for certain sentences. The content, however, was subsequently rewritten and finalized by the authors.

Funding This work was supported by NeuroCure SPARK BIH 2020NeuroCure/ SPARK-BIH/BENEFIT (SK), UM1 HG012076 (LSL), the Hector Fellow Academy (LSL), the Paul Ehrlich Foundation (LSL), the EMBO Young Investigator Programme (LSL), an Emmy Noether fellowship (LU 2336/2-1), grants by the German Research Foundation (DFG, LU 2336/3-1, LU 2336/6-1, STA 1586/5-1, TRR241, SFB1588, Heinz Maier-Leibnitz Award to LSL) and the Else-Kröner-Fresenius Stiftung (2020_EKEA.80 to PH). LM-J and CS are participants in the BIH Charité Clinician Scientist Program. ME received funding from DFG under Germany's Excellence Strategy—EXC-2049—390688087, Collaborative Research Center ReTune TRR 295-424778381, Clinical Research Group KFO 5023 BeCAUSE-Y, project 2 EN343/16-1. BMBF, DZNE, DZHK, DZPG, EU, Corona Foundation, and Foundation Leducg.

Competing interests No, there are no competing interests.

Patient consent for publication Not applicable.

Ethics approval This study involves human participants and was approved by the ethics committees of Charité Universitätsmedizin Berlin (EA1/099/17 and EA4/219/21) and registered at the German Clinical Trials Register (DRKS00012668). Participants gave informed consent to participate in the study before taking part.

Provenance and peer review Not commissioned; externally peer reviewed.

Data availability statement Data are available in a public, open access repository. Processed datasets generated in this study (CellRanger outputs) are available via Gene Expression Omnibus (GSE278119). Raw sequences (fastq files) have been submitted to the European Genome-Phenome Archive (EGA), with the accession numbers EGAD50000000857 (scRNA-seq) and EGAD50000000858 (TCR profiling). The code to reanalyze the data is available on the following repository: https://github.com/agiguelay/n_irAEs_reproducibility/. Requests for additional information should be directed to the lead contact.

Supplemental material This content has been supplied by the author(s). It has not been vetted by BMJ Publishing Group Limited (BMJ) and may not have been peer-reviewed. Any opinions or recommendations discussed are solely those of the author(s) and are not endorsed by BMJ. BMJ disclaims all liability and responsibility arising from any reliance placed on the content. Where the content includes any translated material, BMJ does not warrant the accuracy and reliability of the translations (including but not limited to local regulations, clinical guidelines, terminology, drug names and drug dosages), and is not responsible for any error and/or omissions arising from translation and adaptation or otherwise.

Open access This is an open access article distributed in accordance with the Creative Commons Attribution Non Commercial (CC BY-NC 4.0) license, which permits others to distribute, remix, adapt, build upon this work non-commercially, and license their derivative works on different terms, provided the original work is properly cited, appropriate credit is given, any changes made indicated, and the use is non-commercial. See http://creativecommons.org/licenses/by-nc/4.0/.

ORCID iDs

Ambre Manon Giguelay https://orcid.org/0000-0003-0417-1109 Patrick Maschmeyer https://orcid.org/0000-0002-1705-5302 Leonie Müller-Jensen https://orcid.org/0000-0002-6388-9375 Manpreet Meyer https://orcid.org/0009-0004-5700-8529 Petra Huehnchen https://orcid.org/0000-0002-6825-7270 Wolfgang Boehmerle https://orcid.org/0000-0001-7195-3894 Matthias Endres https://orcid.org/0000-0001-6520-3720

REFERENCES

- Sharma P, Goswami S, Raychaudhuri D, et al. Immune checkpoint therapy-current perspectives and future directions. Cell 2023;186:1652–69.
- 2 Wei SC, Duffy CR, Allison JP. Fundamental Mechanisms of Immune Checkpoint Blockade Therapy. *Cancer Discov* 2018;8:1069–86.
- 3 Postow MA, Sidlow R, Hellmann MD. Immune-Related Adverse Events Associated with Immune Checkpoint Blockade. N Engl J Med 2018;378:158–68.
- 4 Farina A, Villagrán-García M, Vogrig A, et al. Neurological adverse events of immune checkpoint inhibitors and the development of paraneoplastic neurological syndromes. *Lancet Neurol* 2024:23:81–94.
- 5 Mikami T, Liaw B, Asada M, et al. Neuroimmunological adverse events associated with immune checkpoint inhibitor: a retrospective, pharmacovigilance study using FAERS database. J Neurooncol 2021:152:135-44.
- 6 Zimmer L, Goldinger SM, Hofmann L, et al. Neurological, respiratory, musculoskeletal, cardiac and ocular side-effects of anti-PD-1 therapy. Eur J Cancer 2016;60:210–25.
- 7 Johnson DB, Nebhan CA, Moslehi JJ, et al. Immune-checkpoint inhibitors: long-term implications of toxicity. Nat Rev Clin Oncol 2022;19:254–67.
- 8 Albarrán V, Chamorro J, Rosero DI, et al. Neurologic Toxicity of Immune Checkpoint Inhibitors: A Review of Literature. Front Pharmacol 2022;13:774170.
- 9 Möhn N, Mahjoub S, Gutzmer R, et al. Diagnosis and Differential Diagnosis of Neurological Adverse Events during Immune Checkpoint Inhibitor Therapy. J Oncol 2020;2020:8865054.
- 10 Lozano AX, Chaudhuri AA, Nene A, et al. T cell characteristics associated with toxicity to immune checkpoint blockade in patients with melanoma. Nat Med 2022;28:353–62.
- 11 Jing Y, Liu J, Ye Y, et al. Multi-omics prediction of immune-related adverse events during checkpoint immunotherapy. Nat Commun 2020:11:4946.
- 12 Bukhari S, Henick BS, Winchester RJ, et al. Single-cell RNA sequencing reveals distinct T cell populations in immunerelated adverse events of checkpoint inhibitors. Cell Rep Med 2023:4:100868.
- 13 Johnson DB, McDonnell WJ, Gonzalez-Ericsson PI, et al. A case report of clonal EBV-like memory CD4⁺ T cell activation in fatal checkpoint inhibitor-induced encephalitis. Nat Med 2019:25:1243–50.
- Müller-Jensen L, Schulz AR, Mei HE, et al. Immune signatures of checkpoint inhibitor-induced autoimmunity-A focus on neurotoxicity. Neuro Oncol 2024;26:279–94.
- 15 Guidon AC, Burton LB, Chwalisz BK, et al. Consensus disease definitions for neurologic immune-related adverse events of immune checkpoint inhibitors. J Immunother Cancer 2021;9:e002890.
- 16 Hao Y, Hao S, Andersen-Nissen E, et al. Integrated analysis of multimodal single-cell data. Cell 2021;184:3573–87.
- 17 McGinnis CS, Murrow LM, Gartner ZJ. DoubletFinder: Doublet Detection in Single-Cell RNA Sequencing Data Using Artificial Nearest Neighbors. Cell Syst 2019;8:329–37.
- 18 Street K, Risso D, Fletcher RB, et al. Slingshot: cell lineage and pseudotime inference for single-cell transcriptomics. BMC Genomics 2018;19:477.
- 19 Aibar S, et al. SCENIC: single-cell regulatory network inference and clustering. Nat Methods 2017;14:1083–6.
- 20 Elm E von, Altman DG, Egger M, et al. Strengthening the reporting of observational studies in epidemiology (STROBE) statement: guidelines for reporting observational studies. BMJ 2007;335:806–8.
- 21 Subudhi SK, Aparicio A, Gao J, et al. Clonal expansion of CD8 T cells in the systemic circulation precedes development of ipilimumabinduced toxicities. Proc Natl Acad Sci U S A 2016;113:11919–24.
- 22 Cibrián D, Sánchez-Madrid F. CD69: from activation marker to metabolic gatekeeper. Eur J Immunol 2017;47:946–53.
- 23 Matsushima GK, Itoh-Lindstrom Y, P-Y Ting J. Activation of the HLA-DRA Gene in Primary Human T Lymphocytes: Novel Usage of TATA and the X and Y Promoter Elements. Mol Cell Biol 1992;12:5610–9.
- 24 Nakaya M, Xiao Y, Zhou X, et al. Inflammatory T cell responses rely on amino acid transporter ASCT2 facilitation of glutamine uptake and mTORC1 kinase activation. *Immunity* 2014;40:692–705.



- 25 Zhang Y, Reynolds JM, Chang SH, et al. MKP-1 Is Necessary for T Cell Activation and Function. *Journal of Biological Chemistry* 2009;284:30815–24.
- 26 Gan Y-L, Wang C-Y, He R-H, et al. FKBP51 mediates resilience to inflammation-induced anxiety through regulation of glutamic acid decarboxylase 65 expression in mouse hippocampus. J Neuroinflammation 2022;19:152.
- 27 Argyriou A, Horuluoglu B, Galindo-Feria AS, et al. Single-cell profiling of muscle-infiltrating T cells in idiopathic inflammatory myopathies. EMBO Mol Med 2023;15:e17240.
- 28 Doi Y, Oki S, Ozawa T, et al. Orphan nuclear receptor NR4A2 expressed in T cells from multiple sclerosis mediates production of inflammatory cytokines. Proc Natl Acad Sci U S A 2008;105:8381–6.
- 29 Wang C, Jiang H, Liu H, et al. Isoforsythiaside confers neuroprotection against Alzheimer's disease by attenuating ferroptosis and neuroinflammation in vivo and in vitro. Food Science and Human Wellness 2023;12:1730–42.
- 30 Griffith JW, Sokol CL, Luster AD. Chemokines and chemokine receptors: positioning cells for host defense and immunity. *Annu Rev Immunol* 2014;32:659–702.
- 31 Chen C, Peng J, Ma S, et al. Ribosomal protein S26 serves as a checkpoint of T-cell survival and homeostasis in a p53-dependent manner. Cell Mol Immunol 2021;18:1844–6.
- 32 Xiong X, Zhao Y, Tang F, et al. Ribosomal protein S27-like is a physiological regulator of p53 that suppresses genomic instability and tumorigenesis. Elife 2014;3:e02236.
- 33 Healy JA, Han J-H, Bauché D, et al. Advances in Therapies Targeting Inhibitory Checkpoint Receptors: TIGIT, LAG-3, and Beyond. Annual Review of Cancer Biology 2024;8:115–33.
- 34 Strasser A, Jost PJ, Nagata S. The many roles of FAS receptor signaling in the immune system. *Immunity* 2009;30:180–92.
- 35 Yin Q, Wu L, Han L, et al. Immune-related adverse events of immune checkpoint inhibitors: a review. Front Immunol 2023;14:1167975.
- 36 Wu K, Xia B, Zhang J, et al. Positive Correlation of Peripheral CD8⁺ T Lymphocytes with Immune-Related Adverse Events and Combinational Prognostic Value in Advanced Non-Small Cell Lung Cancer Patients Receiving Immune Checkpoint Inhibitors. Cancers (Basel) 2022;14:3568.

- 37 Yasuda Y, Iwama S, Sugiyama D, et al. CD4⁺ T cells are essential for the development of destructive thyroiditis induced by anti-PD-1 antibody in thyroglobulin-immunized mice. Sci Transl Med 2021;13:eabb7495.
- 38 Berner F, Bomze D, Diem S, et al. Association of Checkpoint Inhibitor-Induced Toxic Effects With Shared Cancer and Tissue Antigens in Non-Small Cell Lung Cancer. JAMA Oncol 2019;5:1043–7.
- 39 Johnson DB, Balko JM, Compton ML, et al. Fulminant Myocarditis with Combination Immune Checkpoint Blockade. N Engl J Med 2016;375:1749–55.
- 40 Kitano S, Tsuji T, Liu C, et al. Enhancement of tumor-reactive cytotoxic CD4+ T cell responses after ipilimumab treatment in four advanced melanoma patients. Cancer Immunol Res 2013;1:235–44.
- 41 Oh DY, Cham J, Zhang L, et al. Immune Toxicities Elicted by CTLA-4 Blockade in Cancer Patients Are Associated with Early Diversification of the T-cell Repertoire. *Cancer Res* 2017;77:1322–30.
- 42 Cenerenti M, Saillard M, Romero P, et al. The Era of Cytotoxic CD4 T Cells. Front Immunol 2022;13:867189.
- 43 Rodig SJ, Gusenleitner D, Jackson DG, et al. MHC proteins confer differential sensitivity to CTLA-4 and PD-1 blockade in untreated metastatic melanoma. Sci Transl Med 2018;10:eaar3342.
- 44 Thibodeau J, Bourgeois-Daigneault M-C, Lapointe R. Targeting the MHC Class II antigen presentation pathway in cancer immunotherapy. *Oncoimmunology* 2012;1:908–16.
- immunotherapy. Oncoimmunology 2012;1:908–16.
 Cachot A, Bilous M, Liu Y-C, et al. Tumor-specific cytolytic CD4 T cells mediate immunity against human cancer. Sci Adv 2021;7:eabe3348.
- 46 Xie Y, Akpinarli A, Maris C, et al. Naive tumor-specific CD4(+) T cells differentiated in vivo eradicate established melanoma. J Exp Med 2010;207:651–67.
- 47 Peeters LM, Vanheusden M, Somers V, et al. Cytotoxic CD4+ T Cells Drive Multiple Sclerosis Progression. Front Immunol 2017;8:1160.
- 48 Axelrod ML, Meijers WC, Screever EM, et al. T cells specific for α-myosin drive immunotherapy-related myocarditis. Nature New Biol 2022;611:818–26.
- 49 Voskoboinik I, Whisstock JC, Trapani JA. Perforin and granzymes: function, dysfunction and human pathology. *Nat Rev Immunol* 2015;15:388–400.